Hollow Nanoparticles

Deutsche Ausgabe: DOI: 10.1002/ange.201505242
Internationale Ausgabe: DOI: 10.1002/anie.201505242

Utilizing Reversible Interactions in Polymeric Nanoparticles To Generate Hollow Metal–Organic Nanoparticles

*Longyu Li, Conghui Yuan, Dongming Zhou, Alexander E. Ribbe, Kevin R. Kittilstved, and S. Thayumanavan**

Abstract: *The use of reversible linkers in polymers has been of interest mainly for biomedical applications. Herein, we present a novel strategy to utilize reversible interactions in polymeric nanoparticles to generate hollow metal–organic nanoparticles (MOPs). These hollow MOPs are synthesized from self-assembled polymeric nanoparticles using a simple metal–comonomer exchange process in a single step. The control over the size of the polymer precursor particles translates into a straightforward opportunity for controlling MOP sizes. The shell thickness of the MOPs could be easily tuned by the concentration of metal ions in solution. The underlying mechanism for the formation of these hollow MOPs has been proposed. Evidence for the generality of the method is provided by its application to a variety of metal ions with different coordination geometries.*

The rapidly developing field of nanotechnology depends on versatile strategies that provide access to the next generation of nanomaterials.[1] The majority of current nanomaterials are either purely inorganic,[2] such as silica nanoparticles and metal and metal–oxide nanocrystals, or purely organic,[3] such as polymer nanoparticles and supramolecular assemblies. There is a recent surge in methods for generating hybrid metal–organic coordination materials constructed from metal ions and polyfunctional organic ligands.[4] By functional group variation within the inorganic or organic building blocks, a diverse range of materials can be prepared, demonstrating the versatility of the method. This chemical design feature has led to opportunities for these materials to be employed in a number of diverse applications, such as catalysis, gas storage, biosensing, and biomedicine.[5]

In all of these applications, hollow nanoparticles have increasingly attracted particular interest because of their low density, high surface area, material economy, and lower cost compared to their solid counterparts.[6–11] Herein, we report a simple, rapid, and robust strategy to prepare hollow metal–organic nanoparticles (MOPs), in which we exploit the reversibility of the polymer backbone linkages through a simple addition of metal ions into a solution of well-defined polymeric nanoparticles. We show that: a) the size of the hollow MOPs can be easily tuned by using precursor organic polymer nanoparticles of different sizes; b) control over the thickness of the nanoparticle walls is achieved by controlling the concentration of metal ions; c) the underlying mechanism for the formation of the hollow MOP is controlled by the relative diffusion of the reactive species in solution versus the substrate polymer nanoparticle; and d) a variety of metal ions with different coordination geometries can give rise to the formation of hollow MOPs, indicating the generality of the method.

Precursor organic boronate nanoparticles (BNP) can be prepared using a simple condensation-driven cooperative polymerization of a bisimido boronic acid (Im-BA) molecule and a bisimido catechol (Im-Ca) molecule in methanol (Figure 1 a).[12] The boronate ester bond can be rendered reversible under a variety of conditions. We first explored the possibility of utilizing the strong interaction between Fe^{3+} species and catechols to interrupt the polymer backbone in the BNP. For this purpose, a calculated amount of $FeCl_3$ was simply added to a methanolic suspension of BNP. After stirring the solution for about 12 h, a solid product was collected by centrifugation and washed with methanol. The reaction scheme for formation of the MOP formation is

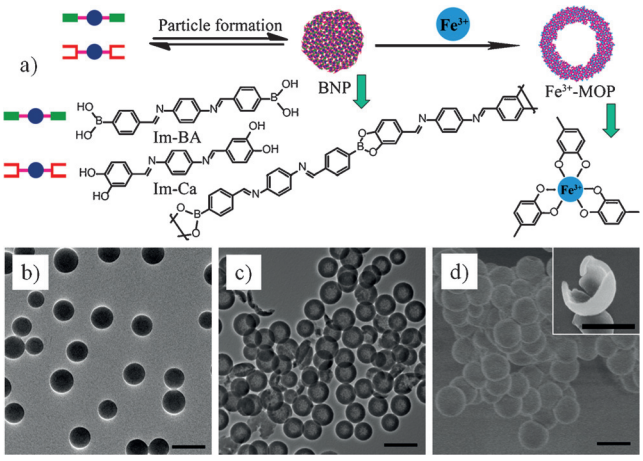

Figure 1. BNP and MOP characterization. a) The syntheses of BNP from Im-Ca and Im-BA and the preparation of hollow MOP by addition of metal chloride salts to the BNP solution. TEM images of b) the BNP and c) the hollow Fe^{3+}-MOP. d) SEM image of the hollow Fe^{3+}-MOP. Inset in (d): SEM image of one broken hollow Fe^{3+}-MOP. Scale bars in (b–d) = 500 nm.

[*] L. Li, Dr. C. Yuan, D. Zhou, Prof. K. R. Kittilstved, Prof. S. Thayumanavan
Department of Chemistry, University of Massachusetts
Amherst, MA 01003-9336 (USA)
E-mail: thai@chem.umass.edu
Dr. C. Yuan
College of Materials, Xiamen University
Xiamen, 361005 (P.R. China)
Dr. A. E. Ribbe
Department of Polymer Science and Engineering
University of Massachusetts, Amherst, MA 01003 (USA)

Supporting information for this article is available on the WWW under http://dx.doi.org/10.1002/anie.201505242.

shown in Figure 1a (the simplicity of the process is also demonstrated in the Supporting Information in Movie S1).

Transmission electron microscopy (TEM) images of BNP with diameters of circa 300 nm are shown in Figure 1b. Upon addition of $FeCl_3$, the color of the solution immediately changed and the formation of nanoparticles with a distinct contrast difference between the center and corona were evident from TEM (Figure 1c). This result provided the first indication of the hollow nature of the resultant nanoparticles. The hollow morphology was further investigated using field emission scanning electron microscopy (SEM; Figure 1d). Broken nanoparticles indeed showed empty inner spaces (inset of Figure 1d), providing direct evidence for the formation of hollow nanoparticles. To test the role of BNP in the formation of hollow MOPs, $FeCl_3$ was added separately into methanolic solutions of Im-Ca and Im-BA (see Figure S1 in the Supporting Information). A significant quantity of precipitated material was observed in the mixture of Im-Ca and $FeCl_3$, in which small nanoparticles were detected using TEM (Figure S2).

The chemical transformation from BNP to MOPs was investigated using energy-filtered transmission electron microscopy (EFTEM). The EFTEM maps show clearly that boron, carbon, nitrogen, and oxygen are all homogenously distributed throughout the entire BNP (Figure 2a and Figure S3). In contrast however, iron was found along with carbon, nitrogen, and oxygen in the hollow nanoparticles (Figure 2b). There was no discernible presence of boron in these particles (Figure S4), supporting our original hypothesis that the hollow nanoparticles might be composed of iron–catechol coordination complexes. To further investigate the hollow nature of these MOPs, EFTEM cross-sectional profiles were analyzed across two individual particles (Figure 2c). Elemental mapping by energy dispersive X-ray absorption spectroscopy (EDS) further confirmed a similar distribution of iron and carbon throughout the entire hollow nanoparticles (Figure S5). The intensity of the mapped images shows the characteristic properties of a hollow structure with contrast between the core and the shell of the nanoparticles.

The versatility of this method to generate hollow MOPs was investigated using other metal ions, specifically Cu^{2+}, Sn^{4+}, and Al^{3+}. These metal ions were chosen because they provide not only variations in their charge, but also in their preferred coordination geometry (4 or 6 coordinate). We investigated whether similar hollow MOP formation could also be observed for these other metal ions. As shown in Figure 2d–f, hollow MOPs are also obtained for all of these ions. EDS analysis of the Sn-based MOP also showed the presence of both tin and carbon in the hollow nanoparticles (Figure S6). NaCl and KCl were also tested and no change was detected for the BNP solutions, indicating that the coordination between the metal ions and catechol groups is important. Additionally, the possibility of preparing hollow dual-metal MOPs was also tested by adding a mixture of $FeCl_3$ and $SnCl_4$ in a 1:1 ratio to the BNP solution. EDS of samples indeed showed a homogenous distribution of the elements Fe and Sn throughout the hollow nanoparticles (Figure S7).

To further confirm that the hollow MOPs are indeed the result of the metal ions forming stable coordination complexes with catechol molecules, electron paramagnetic resonance (EPR) spectroscopy was used to investigate this ligand field environment around the high-spin (hs, d5) Fe^{3+} center. EPR spectroscopy is a sensitive probe of the number of catecholate ligands coordinated to the Fe^{3+} center.[13] Figure 3 shows the EPR spectra of the metal-free BNP and three metal-containing hollow MOPs (containing Fe^{3+}, Al^{3+}, and dual Fe^{3+}–Al^{3+}). The spectrum of as-prepared BNP shows a single sharp feature at $g = 2.00$ that is readily assigned to an organic radical species. The spectrum of the Al^{3+}-containing hollow MOP display the same $g = 2.00$ resonance. However, the spectrum of the Fe^{3+}-based hollow MOP displays two broad features centered at $g' = 4.25$ and about 9.6 in addition to the significantly broadened $g = 2.00$ resonance. These peaks in the spectrum of pure Fe^{3+}-MOPs are rather broad

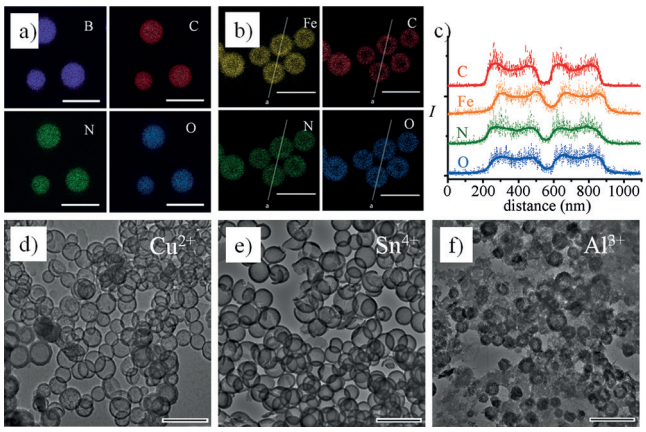

Figure 2. EELS-mapped images of a) BNP (elemental distributions of B, C, N, and O shown) and b) hollow Fe^{3+}-MOP (elemental distributions of Fe, C, N, and O shown). c) Line-scanned EELS profiles of two nanoparticles (taken from Figure 2b) showing the Fe, C, N, and O elemental distributions. TEM images of hollow d) Cu^{2+}-MOP, e) Sn^{4+}-MOP, and f) Al^{3+}-MOP. Scale bars in (a, b, d–f) = 500 nm.

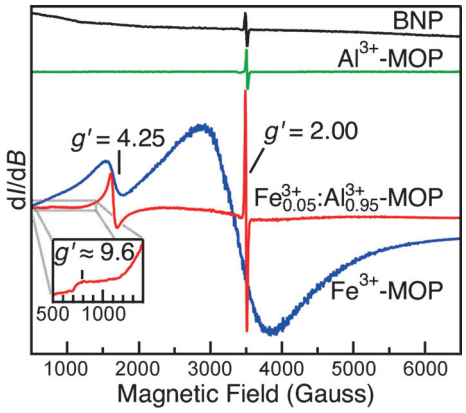

Figure 3. X-band EPR spectra (9.8 GHz; 295 K) of BNP (black), hollow Al^{3+}-MOP (green), hollow Fe^{3+}-MOP (blue), and hollow Fe^{3+}/Al^{3+}-MOP (red; the starting composition was 0.05 mol fraction of $FeCl_3/AlCl_3$). Inset: expanded portion of the spectrum of Fe^{3+}/Al^{3+}-MOP showing the transition at $g' \approx 9.6$.

and indistinguishable from the ferromagnetic resonances that are typical either for Fe_2O_3 nanoparticles[14] or mixed-valent iron centers.[15] To conclusively rule out the formation of these undesired phases, we prepared hollow MOPs using only 5 mol% Fe^{3+} diluted in Al^{3+}. The features in the EPR spectrum of these hollow MOPs, containing diluted Fe^{3+} centers, are much narrower which is consistent with the absence of condensed iron–oxygen phases. Interestingly, an additional weak resonance at $g' \approx 9.6$ is resolved in the spectrum of the Fe^{3+}-doped Al^{3+} hollow MOPs that is occluded by the broad $g' = 4.25$ resonance in the pure Fe^{3+}-containing hollow MOPs. The EPR spectrum of the mixed-metal hollow MOPs displays the same features of Fe^{3+} with tris(catecholate) coordination.[13] The pseudo-octahedral geometry of $[Fe(catecholate)_3]^{3+}$ produces a rhombic EPR spectrum with resonances at $g' = 4.22$ and a weak resonance at $g' \approx 9.6$.[14] In addition to the rhombic Fe^{3+} features at g-values greater than 3, a rather intense radical signal ($g = 2.00$) can also be detected. A similar radical signal was also reported in a paramagnetic Fe^{3+} complex with trisubstituted catecholate ligand DOPA (3,4-dihydroxyphenylalanine).[16]

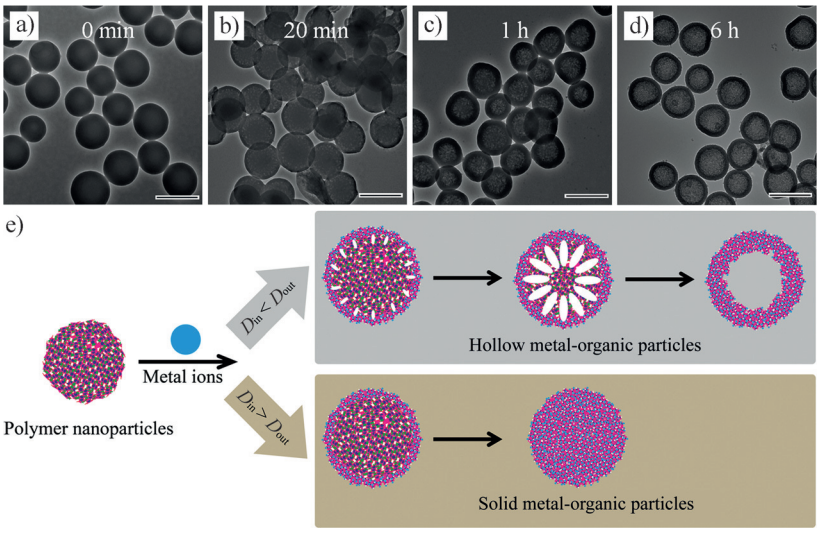

Figure 4. Morphology changes during the hollow particle formation with time. TEM images were taken at a) 0 min, b) 20 min, c) 1 h, and d) 6 h after the addition of $FeCl_3$ into BNP. Scale bar in (a–d) = 500 nm. Conditions: An $FeCl_3$ methanol solution (0.1 mL) was added into a solution of BNP in methanol (1 mL). BNP was prepared from Im-BA and Im-Ca (3 mg mL^{-1} of each) with a ratio of Fe^{3+} ions to Im-Ca of 1:2. Samples for TEM were prepared by drop-casting. e) Schematic illustration showing the transformation of solid polymer nanoparticles to hollow or solid metal–organic particles, depending on the relative diffusivities (D).

To probe the mechanism of the hollow MOP formation, we monitored the temporal evolution of the conversion of the BNPs into hollow MOPs after addition of $FeCl_3$. Aliquots were taken from the reaction mixture at various times and monitored by TEM. A few small cavities in the interior of the solid nanoparticles (Figure 4b) are clearly evident within 20 min. After 1 hour, the particle cores became patchy and concurrently the surface of the nanoparticles became more defined (Figure 4c). Fully hollow nanoparticles were formed after 6 h (Figure 4d) and no further evolution of morphology was detected after 19 h (Figure S8), suggesting that hollow nanoparticles were formed stably in solution. A similar trend in the temporal evolution was also detected for the Sn^{4+}-based hollow MOPs (Figure S9). A reasonable hypothesis is that the formation of hollow MOPs is controlled by the relative diffusion of the reactive species onto the surface of the nanoparticle, which form the interface between the reacting species. Such a mechanistic possibility is reminiscent of the Kirkendall effect, albeit in a very different format, which has been utilized in metallurgy and hollow inorganic oxides and sulfides.[17,18]

Understanding the operating mechanism for hollow MOP formation should allow additional control elements to be introduced. The proposed mechanism for the formation of hollow MOPs would suggest that the diffusion of the boronate ester polymer to the surface of the nanoparticle, where the reaction between Fe^{3+} centers and the boronate ester takes place, is faster than the diffusion of Fe^{3+} from the solution to the interior of the particle (Figure 4e). If the opposite were true (diffusion of Fe^{3+} into the interior of the BNP is faster than outwards diffusion of the boronate ester polymer), then the resultant product would be a solid nanoparticle. We hypothesized then that one can gain control over the thickness of the shell in the hollow MOPs by simply tuning the concentration of Fe^{3+} ions in solution, as these variations will generate an intermediate scenario between that for the solid and the hollow nanoparticles. Accordingly, the ratio of metal ions to the polymer repeat units was varied. Indeed, this variation was found to affect not only the thickness of the shells, but understandably also the rate of the formation of the hollow MOPs. For example, when the concentration of $FeCl_3$ is one eighth of that of the Im-Ca repeat unit in the polymer, it took more than 12 h to complete the formation of hollow MOP. However, this process was completed within 2 h when this ratio was changed to 1:2. As anticipated, the thickness of the shell was also shown to increase consistently with the increasing ratio of $FeCl_3$:Im-Ca, from about 15 nm to 90 nm when the ratio increased from 1:8 to 3:4 (Figure 5a–c). Similar to that observed for Fe^{3+} ions, both the rate of formation and the thickness of the shell increase with increasing the amount of Sn^{4+} ions (Figure S10). The formation of solid MOPs in the presence of an even higher concentration of Fe^{3+} ions (ratio of $FeCl_3$:Im-Ca 1:1) further supports the proposed mechanism. EDS analysis of the samples showed a homogenous distribution of the element Fe in the respective solid nanoparticles (Figure 5d–f).

Finally, it is also important to identify whether the starting size of the boronate nanoparticle is preserved during the transformation to hollow MOPs. The BNP size can be tuned by simply varying the concentration of the monomers.[12] Three BNPs with diameters of 210, 410, and 550 nm were used for the formation of hollow MOPs (Figure S11). Our results indeed show that the resulting size of the hollow MOPs depends on the size of the primary BNP (Figure 5g–i).

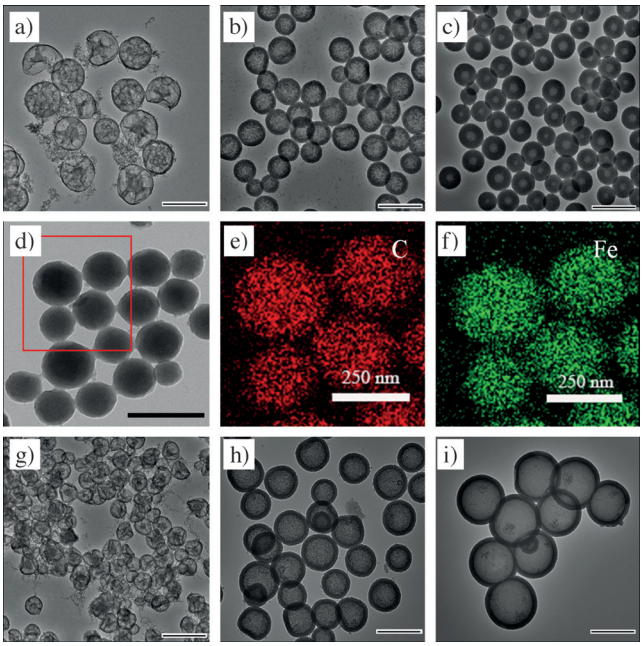

Figure 5. TEM images showing changes in the shell thickness by changing the ratio of Fe^{3+} ions to Im-Ca from a) 1:8, to b) 1:2, to c) 3:4. d) Increasing the ratio to 1:1 led to the formation of solid MOPs. EDS maps of solid Fe^{3+}-MOP showing e) carbon and f) Fe distributions. The size of the hollow MOP was varied by using different BNP sizes from g) 210 nm BNP (using 1.5 mg mL^{-1} monomers), h) 410 nm BNP (using 3.0 mg mL^{-1} monomers), to i) 550 nm BNP (using 5.0 mg mL^{-1} monomers). In (g–i), the ratio of Fe^{3+} ions to Im-Ca was 1:2. Scale bars in (a–d) and (g–i) = 500 nm; scale bars in (e, f) = 250 nm.

Overall therefore, hollow MOPs can be obtained with excellent control over both particle size and shell thickness.

To demonstrate a potential application of these hollow MOPs, hollow carbon particles loaded with metal nanoparticles (M@C) were prepared by direct pyrolysis of hollow Fe^{3+}-MOPs. The advantage of such a system is that the hollow nature of the particles allows for molecular diffusion, while confining the metal nanoparticles within them. To demonstrate such a possibility, hollow Fe^{3+}-MOPs were thermally treated at 800 °C under a N_2 atmosphere for 1 hour, resulting in the formation of light-colored hollow carbon spheres loaded with small dark nanoparticles as shown in the TEM in Figure 6a. The iron content of the small nanoparticles was confirmed from the EDX line scanning data (Figure S12). These small nanoparticles can be removed by the addition of hydrogen chloride with the formation of small bubbles in the solution (Figure 6b), further indicating that these small nanoparticles are likely to be pure Fe nanoparticles. These carbon particles with encapsulated magnetic-Fe nanoparticles have been successfully used as a magnetically separable adsorbent for removing organic waste from aqueous solution using an organic dye (methylene blue, denoted MB).[19] The photograph in Figure 6c and the UV/Vis absorption spectra in Figure 6d demonstrate the separation of MB using these hollow Fe@C nanoparticles. UV/Vis absorption spectra, measured before and after mixing aqueous solutions of MB with Fe@C nanoparticles, indicate that MB has been almost quantitatively removed from the solution (Figure 6d). The

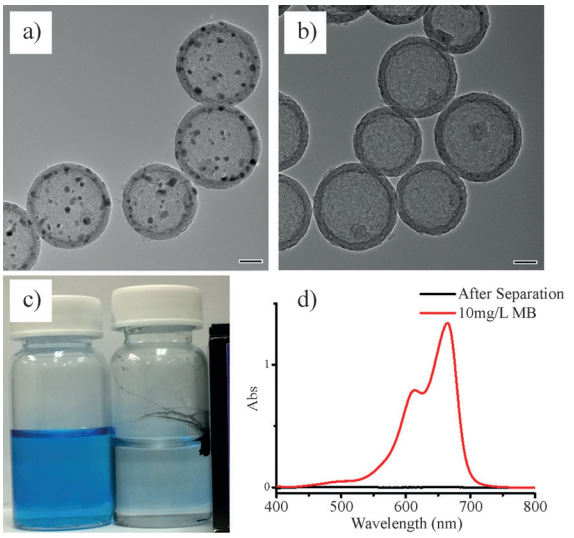

Figure 6. TEM images showing a) hollow Fe@C particles formed after heat treatment of MOPs and b) hollow carbon particles after acid treatment of Fe@C. c) Photograph of the MB solution without (left) and with (right) added Fe@C applying an external magnet. d) UV/Vis absorption spectra before and after the magnetic separation.

magnetic properties of the Fe@C particles are then used to remove them from the aqueous solution. Redistribution of these particles in methanol releases the MB into methanol, which allows for the particles to be reused.

In conclusion, a simple and versatile strategy to prepare hollow metal–organic nanoparticles has been developed in which metal ions are simply added into solutions of solid organic nanoparticles based on boronate esters. The size of the hollow MOPs is dictated by the size of the precursor BNP, which itself exhibits excellent tunability. The formation of these hollow MOPs seem to be independent of the valence and the geometry of the metal ion, which also allows for the incorporation of more than one type of metal ion into the MOPs. Interestingly, the underlying mechanism for the formation of these hollow MOPs seems to be controlled by the diffusion of the reactive species to the interface between the particle and the solution. This understanding of the mechanism allows us to control the shell thickness of the MOPs. Overall, the method reported herein for the controlled preparation of hollow MOPs is highly versatile and may be important for numerous applications, such as catalysis, sensing, storage, and biomedicine, as this approach is extendable to other metal ions and potentially to other organic–inorganic molecular architectures. Moreover, the fields of polymer synthesis and self-assembly are orthogonally and rapidly evolving, both in terms of versatility and new control elements.[20] Our ability to reliably generate hollow organic–inorganic hybrid nanoparticles using polymeric nanostructured templates may be important for the development of nanotechnology based on hybrid materials.

Acknowledgements

We thank the Army Research Office (63889-CH), the National Science Foundation (CHE-1307118), and the

Center for Hierarchical Manufacturing (CMMI-0531171) for funding. The UMass EPR facility was purchased with funds provided by the NSF (CHE-0443180).

Keywords: electron microscopy · hollow nanoparticles · organic–inorganic hybrid composites · polymeric nanoparticles · self-assembly

How to cite: *Angew. Chem. Int. Ed.* **2015**, *54*, 12991 – 12995
Angew. Chem. **2015**, *127*, 13183 – 13187

[1] a) C. R. Martin, *Science* **1994**, *266*, 1961 – 1966; b) Y. Huang, X. Duan, Q. Wei, C. M. Lieber, *Science* **2001**, *291*, 630 – 633; c) T. Suteewong, H. Sai, R. Hovden, D. Muller, M. S. Bradbury, S. M. Gruner, U. Wiesner, *Science* **2013**, *340*, 337 – 341.

[2] a) X. Wang, J. Zhuang, Q. Peng, Y. Li, *Nature* **2005**, *437*, 121 – 124; b) P. D. Howes, R. Chandrawati, M. M. Stevens, *Science* **2014**, *346*, 1247390.

[3] a) R. Savić, L. Luo, A. Eisenberg, D. Maysinger, *Science* **2003**, *300*, 615 – 618; b) J. T. A. Jones, T. Hasell, X. Wu, J. Bacsa, K. E. Jelfs, M. Schmidtmann, S. Y. Chong, D. J. Adams, A. Trewin, F. Schiffman, F. Cora, B. Slater, A. Steiner, G. M. Day, A. I. Cooper, *Nature* **2011**, *474*, 367 – 371; c) J.-H. Ryu, R. Chacko, S. Jiwpanich, S. Bickerton, R. P. Babu, S. Thayumanavan, *J. Am. Chem. Soc.* **2010**, *132*, 17227 – 17235; d) L. Li, K. Raghupathi, C. Yuan, S. Thayumanavan, *Chem. Sci.* **2013**, *4*, 3654 – 3660.

[4] a) H. Furukawa, K. E. Cordova, M. O'Keeffe, O. M. Yaghi, *Science* **2013**, *341*, 1230444; b) M. Oh, C. A. Mirkin, *Nature* **2005**, *438*, 651 – 654; c) A. M. Spokoyny, D. Kim, A. Sumrein, C. A. Mirkin, *Chem. Soc. Rev.* **2009**, *38*, 1218 – 1227; d) A. Carné, C. Carbonell, I. Imaz, D. Maspoch, *Chem. Soc. Rev.* **2011**, *40*, 291 – 305.

[5] a) J. S. Seo, D. Whang, H. Lee, S. I. Jun, J. Oh, Y. J. Jeon, K. Kim, *Nature* **2000**, *404*, 982 – 986; b) R. Banerjee, A. Phan, B. Wang, C. Knobler, H. Furukawa, M. O'Keeffe, O. M. Yaghi, *Science* **2008**, *319*, 939 – 943; c) P. Horcajada, R. Gref, T. Baati, P. K. Allan, G. Maurin, P. Couvreur, G. Ferey, R. E. Morris, C. Serre, *Chem. Rev.* **2012**, *112*, 1232 – 1268.

[6] R. Ameloot, F. Vermoortele, W. Vanhove, M. B. J. Roeffaers, B. F. Sels, D. E. De Vos, *Nat. Chem.* **2011**, *3*, 382 – 387.

[7] A. Carné-Sánchez, I. Imaz, M. Cano-Sarabia, D. Maspoch, *Nat. Chem.* **2013**, *5*, 203 – 211.

[8] a) M. Pang, A. J. Cairns, Y. Liu, Y. Belmabkhout, H. C. Zeng, M. Eddaoudi, *J. Am. Chem. Soc.* **2013**, *135*, 10234 – 10237; b) Z. Zhang, Y. Chen, S. He, J. Zhang, X. Xu, Y. Yang, F. Nosheen, F. Saleem, W. He, X. Wang, *Angew. Chem. Int. Ed.* **2014**, *53*, 12517 – 12521; *Angew. Chem.* **2014**, *126*, 12725 – 12729.

[9] J. Huo, L. Wang, E. Irran, H. Yu, J. Gao, D. Fan, B. Li, J. Wang, W. Ding, A. M. Amin, C. Li, L. Ma, *Angew. Chem. Int. Ed.* **2010**, *49*, 9237 – 9241; *Angew. Chem.* **2010**, *122*, 9423 – 9427.

[10] a) H. Ejima, J. J. Richardson, K. Liang, J. P. Best, M. P. van Koeverden, G. K. Such, J. Cui, F. Caruso, *Science* **2013**, *341*, 154 – 157; b) Z. Zhang, Y. Chen, X. Xu, J. Zhang, G. Xiang, W. He, X. Wang, *Angew. Chem. Int. Ed.* **2014**, *53*, 429 – 433; *Angew. Chem.* **2014**, *126*, 439 – 443; c) F. Zhang, Y. Wei, X. Wu, H. Jiang, W. Wang, H. Li, *J. Am. Chem. Soc.* **2014**, *136*, 13963 – 13966.

[11] a) F. Caruso, R. A. Caruso, H. Möhwald, *Science* **1998**, *282*, 1111 – 1114; b) Y. Yin, R. M. Rioux, C. K. Erdonmez, S. Hughes, G. A. Somorjai, A. P. Alivisatos, *Science* **2004**, *304*, 711 – 714; c) M. H. Oh, T. Yu, S.-H. Yu, B. Lim, K.-T. Ko, M.-G. Willinger, D.-H. Seo, B. H. Kim, M. G. Cho, J.-H. Park, *Science* **2013**, *340*, 964 – 968; d) X. W. Lou, Y. Wang, C. Yuan, J. Y. Lee, L. A. Archer, *Adv. Mater.* **2006**, *18*, 2325 – 2329.

[12] L. Li, C. Yuan, L. Dai, S. Thayumanavan, *Macromolecules* **2014**, *47*, 5869 – 5876.

[13] J. T. Weisser, M. J. Nilges, M. J. Sever, J. J. Wilker, *Inorg. Chem.* **2006**, *45*, 7736 – 7747.

[14] Y. A. Koksharov, S. P. Gubin, I. D. Kosobudsky, M. Beltran, Y. Khodorkovsky, A. M. Tishin, *J. Appl. Phys.* **2000**, *88*, 1587 – 1592.

[15] V. N. Nikiforov, Y. A. Koksharov, S. N. Polyakov, A. P. Malakho, A. V. Volkov, M. A. Moskvina, G. B. Khomutov, V. Y. Irkhin, *J. Alloys Compd.* **2013**, *569*, 58 – 61.

[16] a) M. J. Sever, J. T. Weisser, J. Monahan, S. Srinivasan, J. J. Wilker, *Angew. Chem. Int. Ed.* **2004**, *43*, 448 – 450; *Angew. Chem.* **2004**, *116*, 454 – 456; b) M. J. Sever, J. J. Wilker, *Dalton Trans.* **2006**, 813 – 822.

[17] E. Kirkendall, *AIME Trans.* **1942**, *147*, 104 – 109.

[18] Y. Yin, C. K. Erdonmez, A. Cabot, S. Hughes, A. P. Alivisatos, *Adv. Funct. Mater.* **2006**, *16*, 1389 – 1399.

[19] H. J. Lee, S. Choi, M. Oh, *Chem. Commun.* **2014**, *50*, 4492 – 4495.

[20] C. J. Hawker, K. L. Wooley, *Science* **2005**, *309*, 1200 – 1205.

Received: June 9, 2015
Revised: July 2, 2015
Published online: September 9, 2015

